Title

Degradation of contaminants of emerging concern by UV/H2O2 for water reuse: Kinetics, mechanisms, and cytotoxicity analysis

Authors

Huang, Ying
Kong, Minghao
Coffin, Scott
et al.

Publication Date

2020-05-01

DOI

10.1016/j.watres.2020.115587

Peer reviewed

Water Research 174 (2020) 115587

Contents lists available at ScienceDirect

Water Research

journal homepage: www.elsevier.com/locate/watres

Degradation of contaminants of emerging concern by UV/H_2O_2 for water reuse: Kinetics, mechanisms, and cytotoxicity analysis

Ying Huang [a, b], Minghao Kong [a], Scott Coffin [c, e], Kristin H. Cochran [d], Danielle C. Westerman [d], Daniel Schlenk [c, f], Susan D. Richardson [d], Lecheng Lei [b], Dionysios D. Dionysiou [a, *]

[a] Department of Chemical and Environmental Engineering, University of Cincinnati, Cincinnati, OH, 45221, United States
[b] College of Chemical and Biological Engineering, Key Laboratory of Biomass Chemical Engineering of Ministry of Education, Zhejiang University, Zhejiang, 310012, China
[c] Department of Environmental Sciences, University of California, Riverside, CA, 92521, United States
[d] Department of Chemistry and Biochemistry, University of South Carolina, Columbia, SC, 29208, United States
[e] California State Water Resources Control Board, Sacramento, CA, 95814, United States
[f] Institute of Environmental Health, College of Environmental and Resource Sciences, Zhejiang University, Hangzhou 310058, China

ARTICLE INFO

Article history:
Received 2 November 2019
Received in revised form
31 January 2020
Accepted 2 February 2020
Available online 4 February 2020

Keywords:
UV/H_2O_2 AOP
Water reuse
Transformation products
Cytotoxicity
Contaminants of emerging concern

ABSTRACT

Advanced oxidation using UV and hydrogen peroxide (UV/H_2O_2) has been widely applied to degrade contaminants of emerging concern (CECs) in wastewater for water reuse. This study investigated the degradation kinetics of mixed CECs by UV/H_2O_2 under variable H_2O_2 doses, including bisphenol A, estrone, diclofenac, ibuprofen, and triclosan. Reverse osmosis (RO) treated water samples from Orange County Water District's Groundwater Replenishment System (GWRS) potable reuse project were collected on different dates and utilized as reaction matrices with spiked additions of chemicals (CECs and H_2O_2) to assess the application of UV/H_2O_2. Possible degradation pathways of selected CECs were proposed based on high resolution mass spectrometry identification of transformation products (TPs). Toxicity assessments included cytotoxicity, aryl hydrocarbon receptor-binding activity, and estrogen receptor-binding activity, in order to evaluate potential environmental impacts resulting from CEC degradation by UV/H_2O_2. Cytotoxicity and estrogenic activity were significantly reduced during the degradation of mixed CECs in Milli-Q water by UV/H_2O_2 with high UV fluence (3200 mJ cm^{-2}). However, in GWRS RO-treated water samples collected in April 2017, the cytotoxicity and estrogen activity of spiked CEC-mixture after UV/H_2O_2 treatment were not significantly eliminated; this might be due to the high concentration of target CEC and their TPs, which was possibly affected by the varied quality of the secondary treatment influent at this facility such as sewer-shed and wastewater discharges. This study aimed to provide insight on the impacts of post-UV/H_2O_2 CECs and TPs on human and ecological health at cellular level.

1. Introduction

Wastewater reuse has been increasingly utilized globally to alleviate water shortages, especially in regions with heightened water scarcity (Binz et al., 2016). In typical wastewater treatment trains for potable reuse, microfiltration (MF) or ultrafiltration (UF) are used to remove microorganisms and colloidal particles, and reverse osmosis (RO) is utilized to reject viruses, salts and small molecules, and is often followed by a UV/hydrogen peroxide advanced oxidation process (UV/H_2O_2 AOP) for disinfection and destruction of remaining contaminants of emerging concern (CECs) (Chuang et al., 2017; Patton et al., 2018). A serious limitation for water reuse is the incomplete removal of certain organic contaminants by conventional wastewater treatment, resulting in the presence of many contaminants in the source water to the AOP, including pharmaceuticals, antibacterial compounds, hormones, and plasticizers (Wols et al., 2013). A list of CECs was recommended by a State of California expert panel for monitoring indirect potable

* Corresponding author.
E-mail address: dionysios.d.dionysiou@uc.edu (D.D. Dionysiou).

https://doi.org/10.1016/j.watres.2020.115587
0043-1354/

and non-potable water reuse (Anderson, 2010) as well as aquatic ecosystems (Maruya et al., 2014). According to the list, the targeted CECs in this project were selected based on toxicity, environmental concentration, and persistence through conventional wastewater treatment processes (Anderson, 2010; Maruya et al., 2014).

UV/H_2O_2 is the most widespread UV/AOP implemented and studied for water reuse due to the efficient generation of hydroxyl radicals ($^{\bullet}OH$) (E^0 = 2.4–2.7 V) (He et al., 2014). UV/H_2O_2 is promising for degrading harmful contaminants (Gligorovski et al., 2015; Huang et al., 2018c; Patton et al., 2018; Wols et al., 2013); however, there is less information on the degradation kinetics of priority CECs in real-world mixtures and in the presence of other contaminants (Shu et al., 2016; Wols et al., 2013).

Moreover, organic transformation products (TPs) formed during UV/AOP treatment of wastewater are potentially more toxic than the parent compounds (de Luna et al., 2014; Li et al., 2018; Mariani et al., 2015). Previous studies have used aquatic organisms (e.g. *Daphnia similis* and *Carassius auratus* L.) (de Luna et al., 2014; Shu et al., 2016), microorganisms (e.g. *V. fischeri*) (Olmez-Hanci et al., 2015; Yin et al., 2018), and prediction models (e.g. ECOSAR program) (Gao et al., 2014; Yin et al., 2018) to assess toxicity during advanced oxidation degradation of CECs, providing limited information of the effects on human and ecological health at the cellular level. Thus, cytotoxicity analysis using human cell lines and measurement of the molecular initiating events are important to provide highly relevant information regarding the toxic effects of post-AOP chemicals on humans and wildlife (Huang et al., 2018b; Li et al., 2018; Moussavi et al., 2018). TP determinations from selected CECs via UV/H_2O_2 is also useful for degradation mechanism elucidation alongside supporting toxicity analysis.

The goal of this research is to comprehensively assess the application of UV/H_2O_2 to remove multiple CECs for water reuse, including bisphenol A (BPA), diclofenac (DCF), ibuprofen (IBP), triclosan (TCS), and estrone (E1). The first objective of this study was to explore the degradation kinetics of CEC mixtures by UV/H_2O_2, spiked in Milli-Q water or RO permeate from the GWRS project. Second, TPs formed during single CEC degradation by UV/H_2O_2 were measured and degradation pathways formulated. Third, resulting toxicity during CEC degradation by UV/H_2O_2 was evaluated, spiked in Milli-Q water or RO permeate from GWRS, to provide insights on the impacts of post-UV/H_2O_2 CECs and TPs on human and ecological health at the cellular level.

2. Materials and methods

2.1. Chemicals

Analytical standards of CECs at the highest available purity were purchased from Sigma-Aldrich. Their structures and properties are listed in Table S1. The RO-treated water samples were collected by GWRS staff, and the general water quality parameters are summarized in Table S2. RO permeate collected on April 25, August 7, and October 30, 2017 are marked as RO I, RO II, and RO III, respectively. The water samples were filtered by 0.45 μm glass fiber filters (Whatman) once received and always kept at 4 °C except during experiments. Other chemicals and reagents used are shown in Text S1.

2.2. Analysis methods

Concentrations of CECs were measured by an Agilent 1100 high performance liquid chromatograph (HPLC) with detailed methods in Text S2. Monochloramine (NH_2Cl) concentration was determined using a Hach meter following the indophenol method (Hach Company, 2014). The concentrations of Cl^- were measured using a Dionex ion chromatograph. TPs were detected and analyzed using an ultra-high performanceLC with a quadrupole time-of-flight mass spectrometer (LC-MS) through the collaboration between University of Cincinnati (Agilent 6540) and University of South Carolina (Agilent 6545). Detailed LC-MS and LC-MS/MS conditions are shown in Text S3. Mass spectra were analyzed using Agilent Mass Hunter B.04.00 software.

2.3. Photochemical experiments

Two 15 W low-pressure (LP) mercury UV lamps (Cole-Parmer) or one UV light-emitting diode (LED) lamp (Aquisense Technologies) were used to provide UV photolysis at 254 nm in the experiments. The average UV_{254nm} fluence rate through the reaction solutions was measured by ferrioxalate actinometry and monitored by an ILT1700 calibrated radiometer with an XRD (XRL) 140T254 probe (International Light, Co.), following the methods reported by Bolton et al., (2015) The average UV_{254nm} fluence rate of LP-UV and LED-UV was measured as 0.1 mW cm^{-2} and 0.03 mW cm^{-2}, respectively. The initial concentration of each CEC in the reaction solutions was 1 μM for studying the degradation kinetics and toxicity, while it was 20 μM for analyzing the TPs. 10 mM of phosphate buffer was used to control the pH. In the absence of phosphate buffer, pH of the reaction solutions at the initial timepoint was about 7.7 and pH at endpoints was nearly 7.3, due to the addition of NaOH from the E1 stock solution. RO-treated water samples from GWRS were used as reaction matrices in some experiments with spiked chemicals (CECs and H_2O_2). It should be noted that the concentrations of spiked CECs in the laboratory-scale experiments were significantly higher than typically observed CEC concentrations in RO permeate (when detectable) in order to observe the formed TPs and changes in toxicity in this study. 700–1000 mJ cm^{-2} UV fluence is usually used in full and pilot-scale AOP systems for potable reuse, while much higher UV fluence and H_2O_2 dose are needed in laboratory-scale treatments to minimize the CECs at high concentrations. Typically, CECs, H_2O_2, and Milli-Q water (10 mL of total volume) were spiked into a Petri dish (60 × 15 mm) with a quartz cover (Quartz Scientific Inc., OH), and placed under UV irradiation to initiate reactions. Samples were withdrawn (200 μL) after each UV fluence interval, immediately quenched with 200 μL pure methanol, and analyzed by HPLC. All kinetic experiments were conducted in triplicate at ambient temperature (21 ± 1 °C).

2.4. Cytotoxicity, AhR-binding activity, and ER-binding activity analysis

In this study, cytotoxicity of the samples treated by UV/H_2O_2 was analyzed using the 3-(4,5-dimethylthiazol-2-yl)-2,5-diphenyltetrazolium bromide (MTT) assay in GeneBLAzer CYP1A1-bla LS-180 cells (Life Technologies, CA) (Van de Loosdrecht et al., 1994). The MTT assay has the advantages of rapid response, high precision, and high throughput for determination of cell viability and proliferation, and CYP1A1-bla LS-180 cells provide highly relevant information regarding the cytotoxic effects of chemicals on humans. For the CEC mixture in Milli-Q water, cytotoxicity measurements were also performed with the estrogen receptor (ER) cell line. The % methanol in the control wells was identical to the % methanol in the samples being analyzed. All sample groups were analyzed in triplicate at three concentrations (log M = 5%, 2.5%, and 1%). Absorbance measurements were performed using an automatic microplate reader (SpectraMax+ 384, Molecular Devices, San Jose, CA) at both 595 and 650 nm wavelengths. The ratio of 595/650 nm was then used to compare survival relative to the solvent carrier control wells in each plate, with

normalization to cell-free wells. Values, represented as fraction survival (FS), were calculated through eq. (1) based on a previously reported method (Escher et al., 2014). Samples demonstrating >80% survival relative to solvent control were deemed suitable for agonist-binding assays. Higher values indicate lower cytotoxicity.

$$FS = \frac{Sample595nm/_{650nm} - Control(cell\ free)595nm/_{650nm}}{MeOH\ control595nm/_{650nm} - Control(cell\ free)595nm/_{650nm}} \quad (1)$$

Aryl hydrocarbon receptor (AhR)-binding activity was analyzed using Agonist binding assay and GeneBLAzer CYP1A1-bla-LS180 cells (Invitrogen, Carlsbad, CA). 3,3′,4,4′,5-Pentachlorobiphenyl (PCB-126) was used as the positive control at 12 different concentrations to generate four-parameter Hill Equation standard curves (all $R^2 > 0.99$) per assay batch. The EC_{50} of PCB-126 was 1.7 ng L^{-1} (5.15 pM). The limit of detection (LOD) was 0.2 ng L^{-1} (0.7 pM) and limit of quantification (LOQ) was 0.5 ng L^{-1} (1.6 pM) (Fig. S1). All extracts were analyzed in triplicate.

ER-binding activity was evaluated in the recombinant cell line Vm7Luc4E2, which was prepared following the methods developed by Dr. Denison (Rogers and Denison, 2000). The values are described as their % induction relative to the maximum induction by the positive control 17β-estradiol (E2) on the four-parameter Hill Equation non-linear standard curve (%RME2). The EC_{50} of the positive control E2 was 6.9 ng L^{-1} (Fig. S2). The LOD was 1.3 ng L^{-1} and the LOQ was 2.6 ng L^{-1}. Lower values suggest less estrogenic activity. Two-way analysis of variance (ANOVA) was analyzed for each group, with Tukey's post-hoc ($\alpha = 0.05$). Detailed information about toxicity analysis can be found in Text S4.

2.5. Calculating the contributions from H_2O_2 oxidation, UV, and ROS

The contributions from H_2O_2 oxidation, UV, and reactive oxygen species (ROS) to the degradation of CECs were calculated following methods previously developed by Wu et al., (2016) using rate constants (Table S1) and measured CEC concentration (Fig. S3). Detailed information can be found in Text S5 and Fig. S4.

3. Results and discussion

3.1. CEC degradation kinetics during UV/H_2O_2 treatment in Milli-Q water

Fig. 1a depicts the UV-fluence-based observed first-order rate constants (k_{obs}) of the degradation of five mixed CECs by UV photolysis, LP-UV/H_2O_2, LED-UV/H_2O_2. H_2O_2 alone could not efficiently remove the selected CECs, and the k_{obs} was in the range of $1.25 \times 10^{-6} - 7.50 \times 10^{-6}$ s^{-1} (Fig. S3). In the absence of H_2O_2, only DCF and TCS could be degraded by UV irradiation at a relatively high rate (5.3×10^{-3} cm^2 mJ^{-1}), with a fractional removal of 58% and 56% at 160 mJ cm^{-2} UV fluence (Fig. S3). With the addition of H_2O_2, the k_{obs} of the five CECs were dramatically enhanced under UV irradiation, which might be attributed to the high yield of $^{\bullet}OH$ and the subsequent generation of other ROS (e.g. $O^{\bullet -}$, $HO_2^{\bullet}$, and $O_2^{\bullet -}$) and their great contributions to CEC degradation (Fig. 1b). In addition, LP-UV/H_2O_2 and LED-UV/H_2O_2 achieved similar removal efficiency of the selected CECs except for DCF, indicating lower intensity illumination systems with larger timescales would not lead to significant differences in degradation kinetics of these CECs.

As H_2O_2 dosage increased from 0.1 to 2 mM (Fig. 1c), k_{obs} of mixed CECs also dramatically increased during UV/H_2O_2 treatment at pH 7.4 in the presence of phosphate buffer. For DCF and TCS, the k_{obs} only increased by a factor of 2.1, but for BPA, E1, and IBP, the k_{obs} notably increased by factors of 7, 5.3, and 6.9, respectively. The experimental results of DCF, BPA, and IBP positively correlated with the prediction by Kwon *el al.* (Kwon et al., 2019), suggesting DCF and TCS are primarily degraded by UV photolysis, while BPA, E1, and IBP are more strongly degraded by ROS.

Changes in reaction pH (5.3–8.5) resulted in different impacts on the degradation of selected CECs by UV/H_2O_2 as shown in Fig. 1d: the k_{obs} of TCS decreased by 28% at pH 5.3–6.6, but increased by 46% at the pH range 6.6–8.5, while the k_{obs} of the other four CECs (BPA, E1, DCF, and IBP) decreased by 18–46% in the mixture. As reported in our previous work (He et al., 2012; Huang et al., 2018c), at high pH, hydroxide scavenges/quenches hydroxyl radicals, leading to theoretically lower reactivity/degradation of the CEC; but with TCS it's shown that the base form (above pKa = 7.9) is degrading faster despite the "quenched" hydroxyl radicals/lack of radicals (Huang et al., 2018c). Therefore, influence of pH on the CEC degradation should be considered based on the chemical properties of target contaminants during the UV/H_2O_2 process and the change of the $^{\bullet}OH$ demand.

3.2. CEC degradation kinetics by UV/H_2O_2 in GWRS RO-treated water

As shown in Fig. 2, the water samples collected on different dates resulted in various effects on the k_{obs} of spiked CECs in the UV/H_2O_2 process despite similar monitored water parameters (Table S2). When reactions in RO I were compared to those in Milli-Q water, there were two different trends within the five spiked CECs: 1) for DCF and TCS, the k_{obs} was moderately decreased in RO I by 32.7% and 36.8%, respectively, which can be attributed to the primary CEC degradation by UV photolysis and lesser influence of ROS-oxidation by the RO I matrix; 2) for BPA, E1, and IBP, the k_{obs} was significantly decreased (86.8%–95.2%), given that ROS-oxidation mainly contributed to the CEC degradation. On the contrary, RO II and RO III showed much less influence on the degradation of spiked CECs (Fig. S5). This result suggests some compounds in RO I that were competing for the ROS, compared to RO II and RO III.

To investigate the reason for the higher ROS demand of RO I, the effects of monitored water parameters on the UV/H_2O_2 processes in Milli-Q water were evaluated separately. The concentrations of these water parameters were chosen based on the maximum values of all real GWRS RO-treated water samples (Table S2). As seen from Figs. S6, 2 mM HCO_3^-, 1 mM NO_3^-, 1 mM Cl^-, and 14.1 μM NH_2Cl did not exhibit significant effects on the CEC degradation in mixture by UV/H_2O_2. The impact of total organic carbon (TOC) in the RO permeate was not evaluated due to the low concentration (0.1 mg L^{-1}) and unknown constituents of the TOC.

Based on the results above, it is hypothesized that the difference in RO permeate collected on different date cannot be captured by the general parameters in Table S2. As reported by Kwon et al., the $^{\bullet}OH$ demand in the Han River was notably elevated with the generation of more low-molecular weight dissolved organic matter (LW-DOM) during the rainy alga season (Seoul, Korea), although DOM concentrations were relatively stable (1.4–2.0 mg L^{-1}) throughout the year (Kwon et al., 2019). LW-DOM would react with $^{\bullet}OH$ at higher rate (Appiani et al., 2014), which could pass through the MF and RO pretreatment (Chuang et al., 2017; Kwon et al., 2019; Patton et al., 2018). Additionally, due to the reactions of chlorine added before MF with the residual/bio-generated ammonia in the wastewater, UV/H_2O_2 in the GWRS RO permeate is actually a *de facto* UV/H_2O_2-chloramines AOP, which are less effective in removing organic contaminants and more susceptible to the DOM (Zhang et al., 2019). Therefore, the higher ROS demand of RO I might be due to the varied quality of sewage and wastewater discharges as secondary treatment influent (i.e. more LW-DOM), but

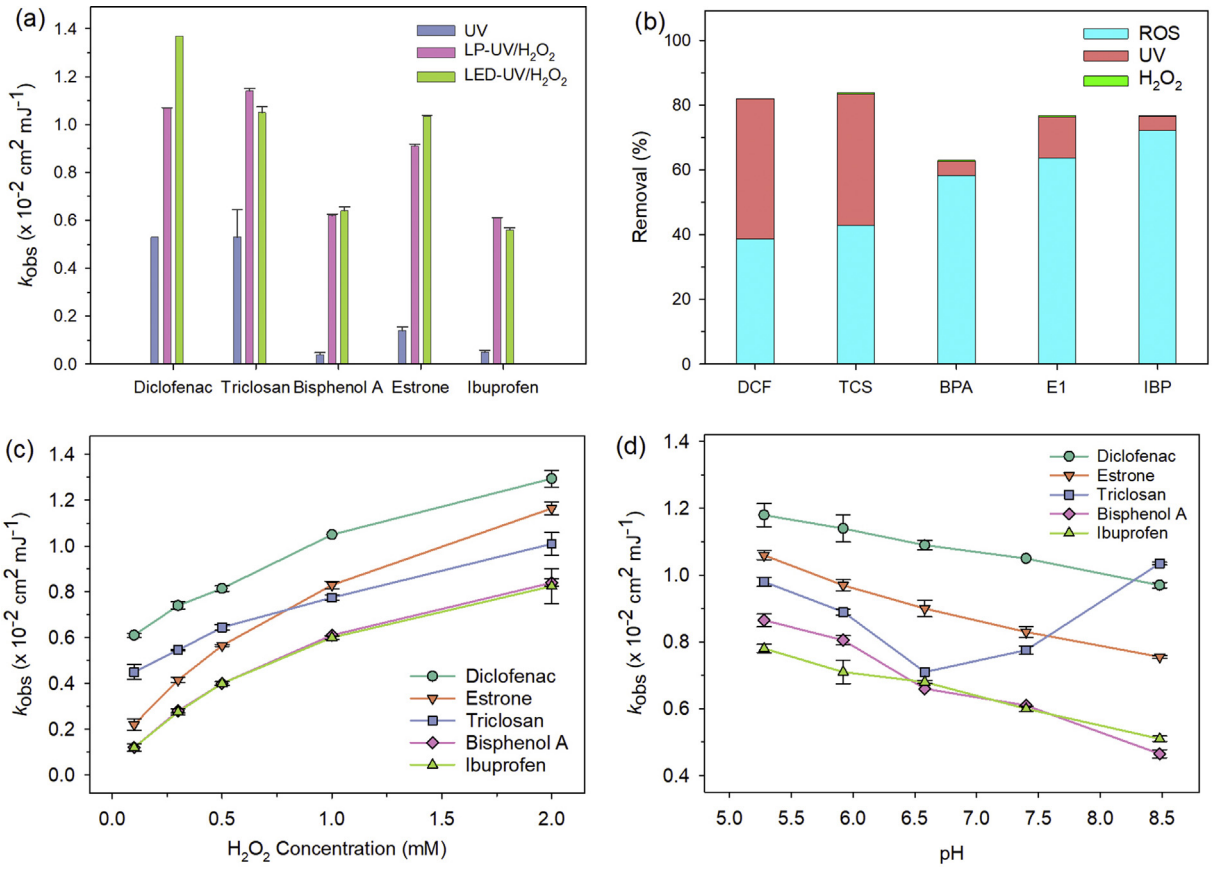

Fig. 1. (a) The k_{obs} of CEC degradation by LP-UV, LP-UV/H_2O_2, and LED-UV/H_2O_2 ($pH_{endpoint}$ = 7.3, no buffer); (b) contributions from H_2O_2, UV, and ROS to the CEC degradation in LP-UV/H_2O_2 at 160 mJ cm^{-2} UV fluence (0.44 h) ($pH_{endpoint}$ = 7.3, no buffer); (c) effects of H_2O_2 dosage (pH was buffered at 7.4) and (d) effects of pH on the k_{obs} of CECs in LP-UV/H_2O_2. UV_{254nm} fluence rate (LP-UV) = 0.1 mW cm^{-2}, UV_{254nm} fluence rate (LED-UV) = 0.03 mW cm^{-2}, $[CEC]_0$ = 1 μM, $[H_2O_2]_0$ = 1 mM, and matrix = Milli-Q water.

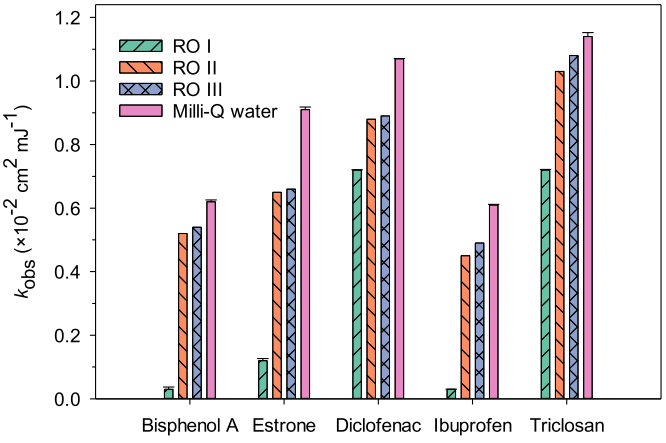

Fig. 2. k_{obs} of spiked CEC degradation in the GWRS RO permeate samples by LP-UV/H_2O_2. UV_{254nm} fluence rate (LP-UV) = 0.1 mW cm^{-2}, $[CEC]_0$ = 1 μM, $[H_2O_2]_0$ = 1 mM, pH_0 = 7.7 (with the spiked CECs), $pH_{endpoint}$ = 7.3.

the specific reason for the quality changes is unknown and not interpreted by the generally monitored parameters, which deserves further investigation in the future.

To further investigate these GWRS water samples (April 25, 2017), the cytotoxicity and ER activity of them were assessed without spiked chemicals. As shown in Fig. S7a, the fraction survival of all original water samples was a little bit lower than the control (either 2.5% or 5% MeOH), indicated possible cytotoxicity of these water samples. For ER-binding activity analysis, estrogen equivalents (EEQ, ng L^{-1}) were calculated for the non-spiked water samples. The mean EEQs of water samples from secondary treatment and microfiltration effluent were below the LOD (1.6 ng L^{-1}), while the mean EEQs of water samples from RO permeate and Santa Ana river were little above the LOD (Fig. S7b). One-way ANOVA was carried out to statistically analyze pure SE, MF, RO, Santa Ana river samples, and their spiked 1 mM H_2O_2 counterparts. ANOVA results ($F_{(7,16)}$ = 7.41, p=0.0005) indicate significant differences exist between eight samples. Turkey's Honest Significant Difference *post-hoc* revealed highly significant differences ($p<0.01$) between RO spiked with 1 mM H_2O_2 and the blanks, as well as MF and SE (Fig. S7b), even though the residual H_2O_2 was quenched by 4 μL catalase (1.28×10^6units/mL) before ER-binding activity analysis. Significant differences between samples are denoted by letters (α=0.05). Relatively high variability in the RO permeate and Santa Ana River estrogenic activity relative to the blank sample should be noted (see error bars in Fig. S7). However, the large uncertainty in the RO permeate and Santa Ana River estrogenic activity relative to the blank sample should be noted (see error bars in Fig. S7). These results indicate that unknown constituents of these water samples possibly pose little cytotoxicity and estrogenic activity. Further research is needed to fully characterize the RO permeate at this facility during different seasons.

3.3. Degradation mechanisms of CECs during UV/H_2O_2 treatment

TPs detected for BPA, DCF, IBP, TCS, and E1 during individual degradation in the UV/H_2O_2 process are summarized in

Tables S3–S7, supported by the UV fluence-dependent evolution of TPs and the MS/MS spectra (with mass measurement accuracy in ppm) as shown in Figs. S8–12. Isomeric structures for certain degradation products were observed at different retention times, which are annotated with lowercase letters (i.e. a and b). There are new tentatively identified TPs with detailed MS/MS spectra, such as B_{245} for BPA and $D_{244(-)}$, ionized via negative ESI, for DCF. The proposed degradation pathways for BPA, DCF, IBP, TCS, and E1 are shown in Figs. 3–7.

As presented in Fig. 3, hydroxylation was the main route for BPA degradation by ROS, producing hydroxylated BPA, $B_{243a\text{-}b}$, and subsequently forming byproducts $B_{259a\text{-}b}$. The proposed structure of $B_{243a\text{-}b}$ ($[M\text{-}H]^-$, *m/z* 243.1021, $C_{15}H_{16}O_3$, 2.5 *ppm*) is supported by the fragment ion *m/z* 149.0592, showing cleavage between the two aromatic rings and corresponding to loss of phenol (Fig. S8). The initial step in hydroxylation is the generation of a carbon centered radical due to •OH addition, followed by oxygen addition, and the subsequent removal of the perhydroxyl radicals (HOO•) (Kang et al., 2018; Wu et al., 2016).

Quinone derivatives were observed during BPA degradation, such as $B_{257a\text{-}b}$, B_{273}, B_{271}, and B_{181}, which were formed after further •OH oxidation of hydroxylation products (Dhara et al., 2016; Gligorovski et al., 2015). Bond breakage occurred adjacent to the methyl bridge of BPA due to •OH oxidation (Li et al., 2017), yielding B_{149}. B_{151} was not observed, most likely due to its rapid oxidation by •OH to generate B_{167} and B_{183}. The proposed structure of B_{167} ($[M\text{-}H]-$, *m/z* 167.0704, $C_9H_{12}O_3$, 6 *ppm*) is supported by the fragment ion *m/z* 149.0608, which is due to the loss of water, a common fragmentation pattern in phenolic compounds (Fig. S8).

B_{245} is a newly identified product, produced by the loss of a central methyl group and hydroxylated on both sides of the parent molecule. The proposed structure of B_{245} ($[M\text{-}H]^-$, *m/z* 245.0817, $C_{14}H_{14}O_4$, 1 *ppm*) is supported by the fragmentation ions *m/z* 227.0712 and *m/z* 109.0317 (Fig. S8). The fragment ion *m/z* 227.0712 is due to loss of water from a phenolic moiety, and the fragment ion *m/z* 109.0317 is due to cleavage between the two aromatic rings and

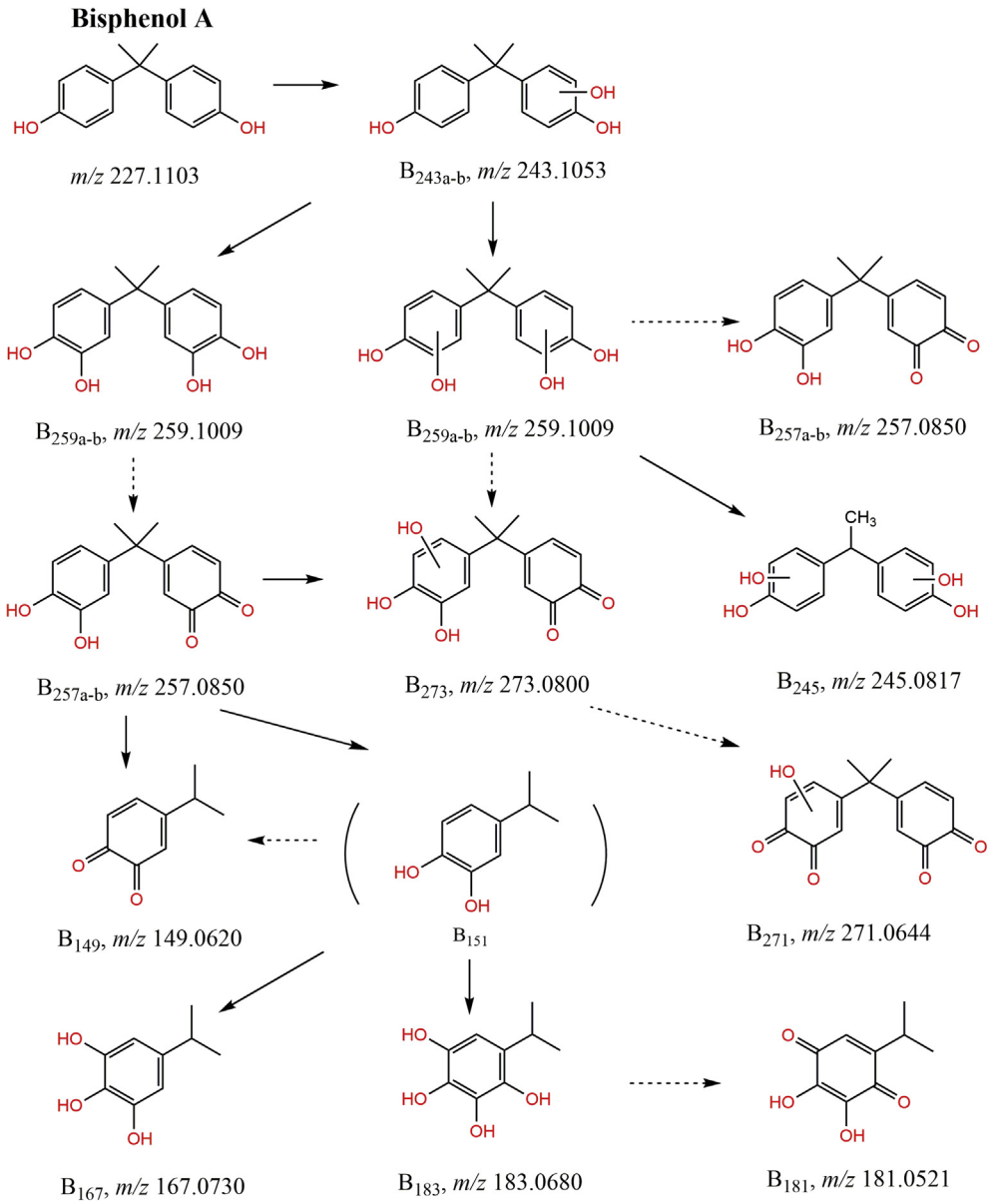

Fig. 3. Possible degradation pathways of BPA in UV/H_2O_2.

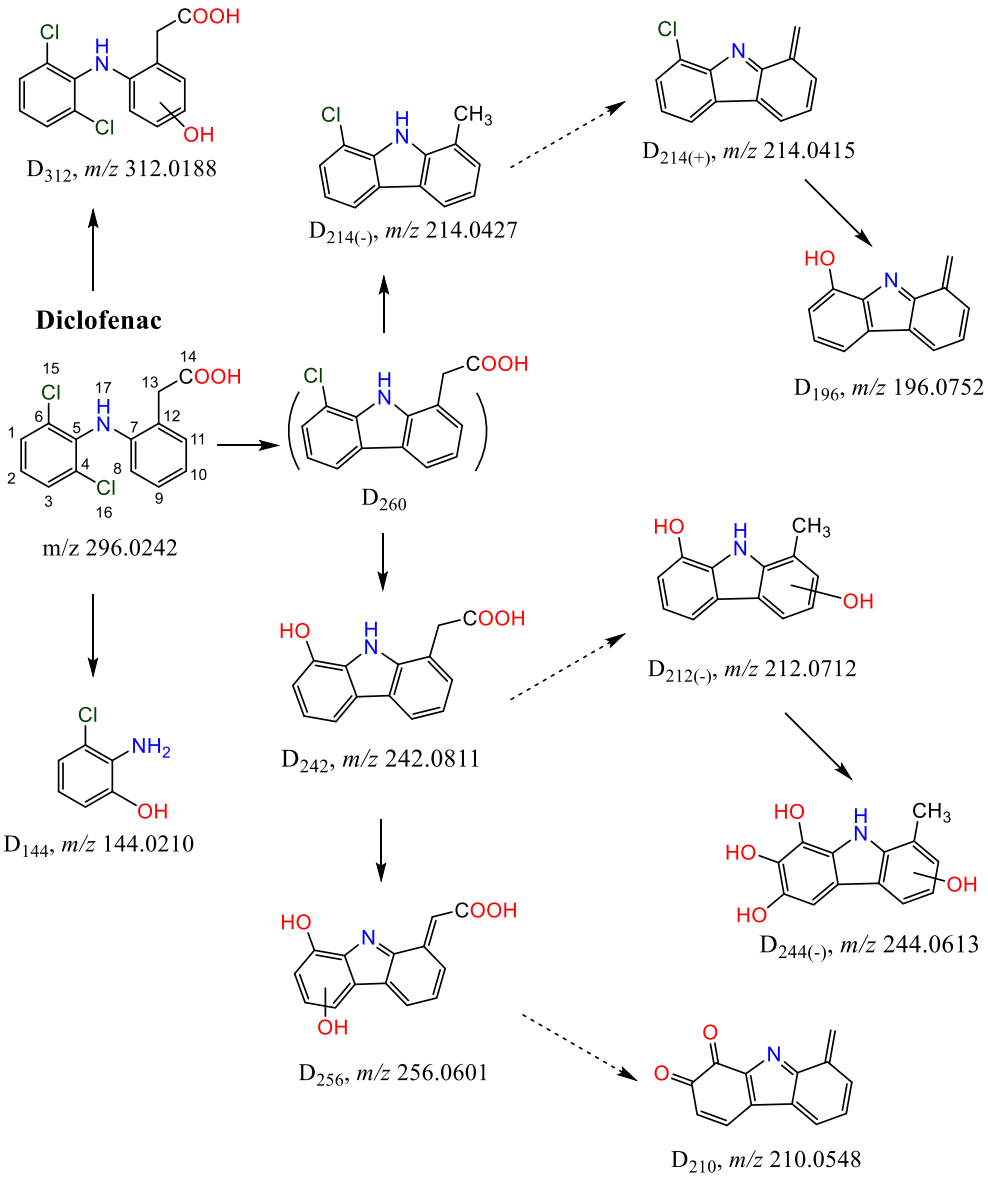

Fig. 4. Possible degradation pathways of DCF in UV/H_2O_2. A (+) or (-) indicates in which ionization mode TP was observed.

corresponding observed dihydroxybenzene. The elimination of the $-CH_3$ group should be attributed to the •OH oxidation of the central C atom on the methyl bridge of BPA, which was also observed during formation of other BPA byproducts, such as 4-hydroxyacetophenone, through •OH-induced oxidation reactions (Abdelraheem et al., 2019).

Due to the complex structure of DCF and the non-selective property of •OH, several degradation routes were observed during DCF degradation in UV/H_2O_2. Direct hydroxylation, dechlorination-hydroxylation, cyclization, and decarboxylation may all occur simultaneously during formation of these TPs (Fig. 4). Direct hydroxylation contributed to the generation of D_{312}, due to the attack on the benzene ring by •OH, as well as in the formation of $D_{212(-)}$, $D_{244(-)}$, and D_{256}. Interestingly, cyclization products were observed during DCF degradation in UV/H_2O_2, namely $D_{214(-)}$, $D_{214(+)}$, $D_{244(-)}$, D_{242}, D_{196}, D_{256}, and $D_{212(-)}$. DCF was in the deprotonated form at the reaction pH, which could spontaneously dechlorinate from its triplet state under UV irradiation, leading to ring closure and forming a five-membered cyclic product D_{260} (Musa and Eriksson, 2009). D_{260} was reported as the primary TP during UV_{254nm} photolysis of DCF (Alharbi et al., 2017), however, it was not observed using UV/H_2O_2 under the current reaction conditions; its absence may be due to its further oxidation by •OH through dechlorination-hydroxylation and decarboxylation routes.

Decarboxylation was initiated with •OH-involved electron transfer on the carboxylic acid of D_{260}/D_{242}, forming a carboxylic radical, which transferred to $D_{214(-)}$/$D_{212(-)}$, followed by the removal of CO_2 and an electron (Pérez-Estrada et al., 2005). The proposed structure of $D_{212(-)}$ ($[M-H]^-$, *m/z* 212.0712, $C_{13}H_{11}NO_2$, 3 *ppm*) is supported by fragment ion *m/z* 194.0576, corresponding to loss of water, which is common in compounds with hydroxyl functional groups (Fig. S9). The observed fragmentation, as well as the $[M-H]^-$ isotopic pattern where the ^{37}Cl isotope can be seen, support the proposed structure of $D_{214(-)}$ ($[M-H]^-$, *m/z* 214.0427, $C_{13}H_{10}ClN$, 1 *ppm*). Fragment ion *m/z* 178.0654 corresponds to loss of HCl, and consequently, the ^{37}Cl isotopic pattern is no longer observed in this fragment (Fig. S9). $D_{214(-)}$ was susceptible to subsequent •OH-oxidation, with the production of a quinone-like

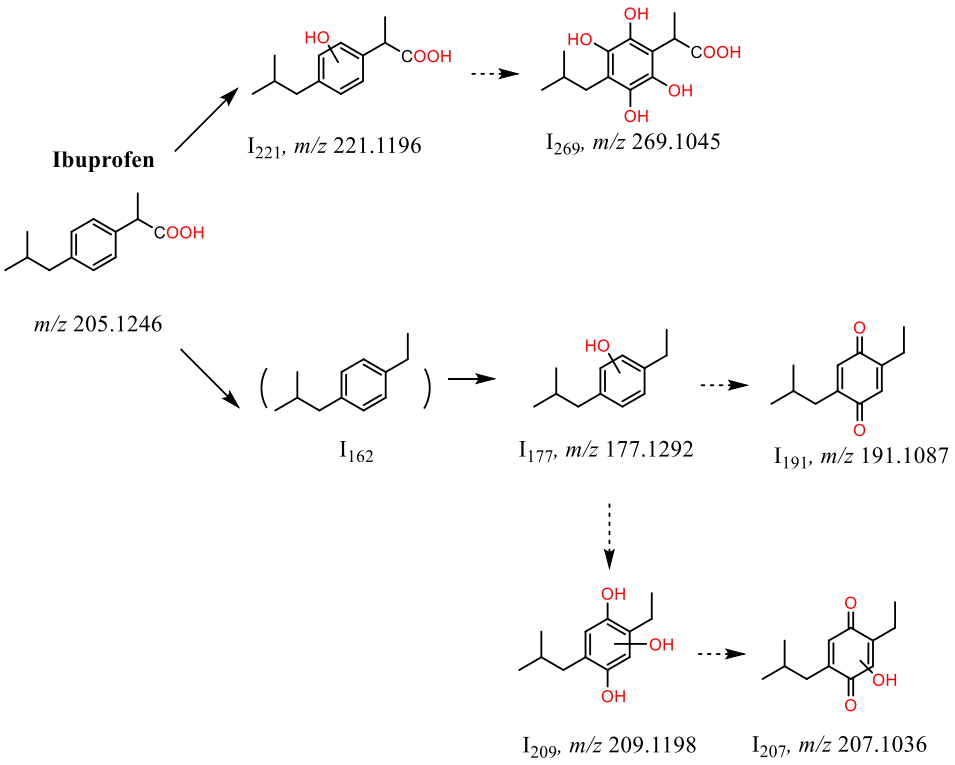

Fig. 5. Possible degradation pathways of IBP in UV/H_2O_2.

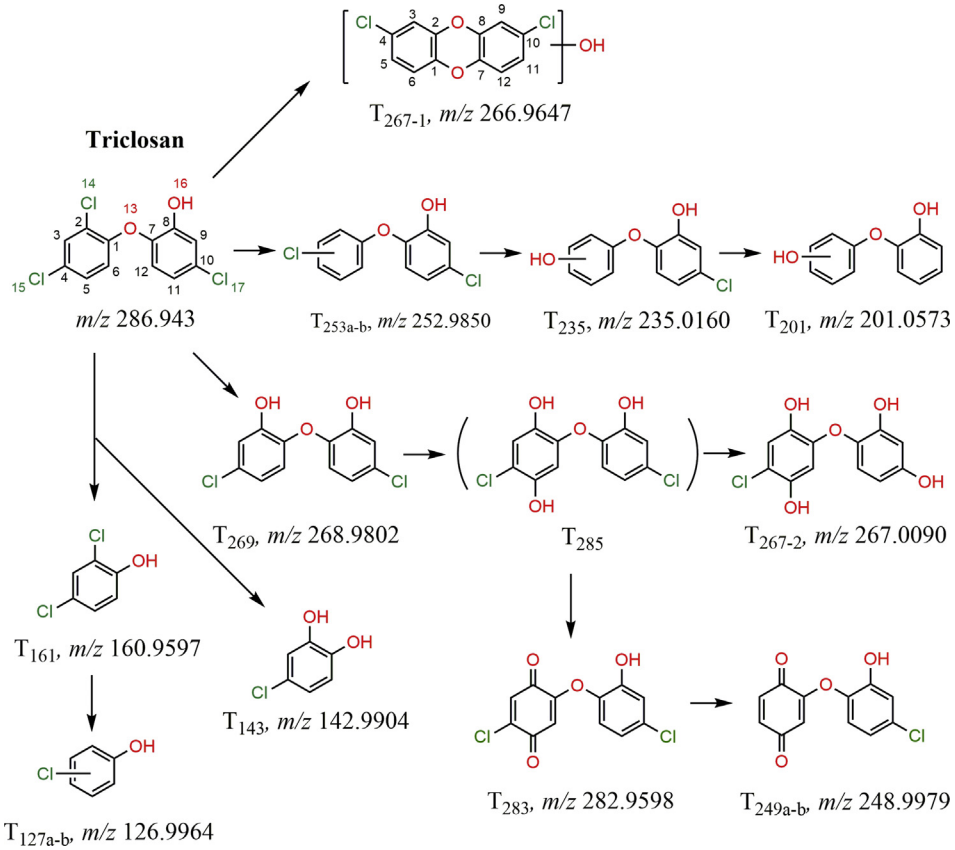

Fig. 6. Possible degradation pathways of TCS in UV/H_2O_2.

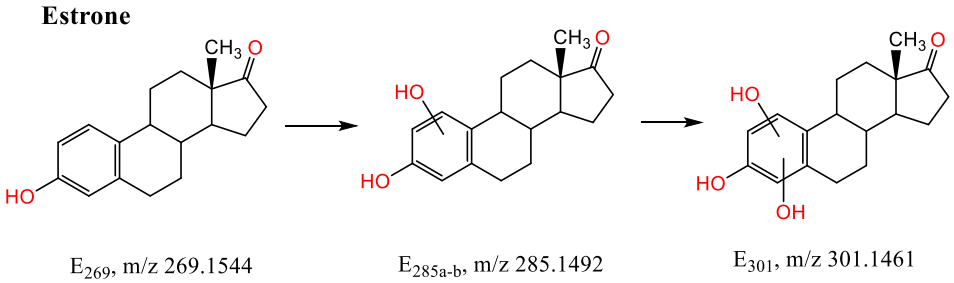

Fig. 7. Possible degradation pathways of E1 in UV/H_2O_2.

product $D_{214(+)}$ (Pérez-Estrada et al., 2005; Sein et al., 2008), and $D_{212(-)}$ could be further oxidized by •OH to form $D_{244(-)}$ through hydroxylation. The proposed structure of $D_{244(-)}$ ([M-H]$^-$, *m/z* 244.0613, $C_{13}H_{11}NO_4$, 1 *ppm*) is supported by two fragment ions at *m/z* 226.0491 and 158.0612, corresponding to loss of water and cleavage of the ring with three hydroxy groups, respectively (Fig. S9).

Dechlorination-hydroxylation was also observed during formation of D_{196} and D_{242}, in which a carbon centered radical was formed through the *ipso*-attack by •OH at the carbon atom of C—Cl group and a subsequent heterolytic cleavage of the C—Cl bond (Huang et al., 2018a; Wu et al., 2016). Direct hydroxylation on D_{242} led to the formation of D_{256}, which could be subsequently oxidized by •OH to yield a quinone derivative D_{210}. The product D_{144} might be produced from the C—NH bridge cleavage on DCF, which was initiated by the •OH attack on DCF's C_5 (Pérez-Estrada et al., 2005; Vogna et al., 2004) and followed by dechlorination-hydroxylation.

During the degradation of IBP, decarboxylation occurred on the carboxylic acid of IBP undergoing a similar route to that of DCF. I_{162} was generated this way before being rapidly oxidized to I_{177}, the most abundant TP (Fig. S10), via hydroxylation on the benzene ring. Hydroxylation was the main mechanism for the •OH-induced oxidation on IBP, as shown in Fig. 5, contributing to the formation of the majority of IBP TPs, such as I_{221}, I_{269}, I_{177}, and I_{209}. With the addition of •OH on the *para*-position to the existing hydroxyl group on the benzene ring of IBP, quinone derivatives I_{191} and I_{207} could be generated from the corresponding hydroxylation products I_{177} and I_{209}.

Detected TPs of TCS are shown in Fig. 6, supported by high resolution-MS and MS/MS spectra presented in Fig. S11. Through a dechlorination-hydrogenation route, T_{253b} was formed as the dominant/most abundant TP at 160 mJ cm^{-2} UV fluence as shown in Fig. S11, which was mainly due to the UV photolysis at 254 nm (Kliegman et al., 2013). This route also contributed to the formation of $T_{127a\text{-}b}$, T_{201}, and $T_{249a\text{-}b}$. Dechlorination-hydroxylation due to •OH-induced *ipso*-attack was observed with the formation of T_{235}, T_{269}, and $T_{267\text{-}2}$. The proposed structure of T_{235} ([M-H]$^-$, *m/z* 235.0160, $C_{12}H_9ClO_3$, 3 *ppm*) is supported by the fragmentation and the [M−H]$^-$ isotopic pattern as shown in Fig. S11: the ^{37}Cl isotope can be seen in the spectrum, and the two fragments, *m/z* 217.0050 and 181.0275, correspond to loss of water and subsequent loss of HCl. The fragment ion showing loss of water and HCl does not display the chlorine isotope pattern, confirming its loss through fragmentation. •OH-addition readily occurred on the *para*-position of the phenolic group of T_{269} (Gao et al., 2014), resulting in T_{285}, which was followed by the rapid •OH-oxidation to form the quinone product T_{283}. Of note, $T_{267\text{-}1}$ is a hydroxylated product of 2,8-dichlorodibenzodioxin (2,8-DCDD), which is a well-known highly toxic compound with AhR activity. 2,8-DCDD, resulted from the cyclization of TCS under UV irradiation, initiated by transferring an electron from the phenolic group to •OH, followed by the removal of a chlorine atom on C_2 and the subsequent recombination of C_2 and C_8 (Kliegman et al., 2013; Latch et al., 2003; Mezcua et al., 2004). The continuous attack of •OH could lead to the breakdown of the ether bond (Munoz et al., 2012), generating T_{161} and T_{143}. The proposed structure of T_{143} ([M-H]$^-$, *m/z* 142.9904, $C_6H_5ClO_2$, 1 *ppm*) is supported by the fragmentation and the [M−H]$^-$ isotopic pattern as shown in Fig. S11, with the ^{37}Cl isotope visible in the mass spectrum. The primary fragment ion (*m/z* 107.0142) corresponds to loss of HCl, consistent with the lack of a chlorine isotope pattern in the fragment ion. The molecular ion also has a negative mass defect, further supporting the presence of chlorine in the molecule, and the positive mass defect on the fragment peak supports the loss of chlorine through fragmentation.

During E1 degradation, only hydroxylation products were observed, $E_{285a\text{-}b}$ and E_{301}, which could be ascribed to the continuous attack of •OH on the phenolic ring (Fig. 7). The proposed structure of E_{285} ([M-H]$^-$, *m/z* 285.1492, $C_{18}H_{22}O_3$, 2 *ppm*) is supported by several fragment ions in the MS/MS spectrum (Fig. S12). Loss of water (*m/z* 267.1388) is consistent with a phenolic moiety. The other three fragments (*m/z*'s 245.1148, 153.0558, and 123.0437) are likely formed by charge-driven rearrangements; commonly, the C- and D-rings of steroids are opened through collision-induced fragmentation (Wooding et al., 2013). The proposed structure of $E_{285a\text{-}b}$ has several possible isomers arising from placement of the additional hydroxyl group on the aromatic ring, which are indistinguishable in the MS/MS spectra in Fig. S12.

3.4. Cytotoxicity, AhR-binding activity, and ER-binding activity analysis

Certain TPs formed in UV-AOPs may pose higher toxicity than the parent compounds (de Luna et al., 2014; Li et al., 2018; Mariani et al., 2015). Consequently, it is important and necessary to assess the toxicity of the treated solution, even though CECs may be effectively removed in the UV/H_2O_2 treatment. It should be noted that the concentrations of spiked CECs in the laboratory-scale experiments were significantly higher than typically observed CEC concentrations in RO permeate (when detectable). This study aimed to assess whether the TPs resulted in a relative increase or decrease in toxicity as determined by corresponding cell-based assays. The relative responses of AhR-binding activity in all tested samples were lower than the LOD (1.7 ng L^{-1}, Fig. S1), suggesting no AhR-binding activity of the treated solution (Figs. S13—S14). Results of cytotoxicity and ER-binding activity are summarized in Tables 1—2 and detailed results are shown in Figs. S15—S22.

3.4.1. Cytotoxicity and ER-binding activity of resulting solutions during the degradation of individual CECs in Milli-Q water by UV/H_2O_2

The cytotoxicity of treated BPA slightly *increased* ($p = 0.741$) with BPA degradation at 640 mJ cm^{-2} UV fluence (Fig. S15);

Table 1
Individual cytotoxicity and ER-binding activity of BPA, IBP, DCF, TCS, and E1 during the LP-UV/H_2O_2 treatment within 640 mJ cm^{-2} UV fluence (1.78 h) in Milli-Q water. UV_{254nm} fluence rate = 0.1 mW cm^{-2}, $[CEC]_0$ = 1 μM, $[H_2O_2]_0$ = 1 mM, $pH_{endpoint}$ = 7.3, no buffer.

CECs	Cytotoxicity			ER-binding activity			ER-binding activity linear trend[b]	
	log M [a]	p		log M	p		p	
Bisphenol A	5%	0.74	Increased	1%	0.04	Increased	0.09	Positive
Diclofenac	1%	<0.0001	Decreased	0.05%	0.001	Increased	–	Positive
Ibuprofen	5%	0.998	Increased	1%	0.15	Decreased	0.36	Negative
Triclosan	5%	0.81	Increased	1%	0.14	Decreased	0.03	Negative
Estrone	5%	0.63	Decreased	1%	0.54	Increased	0.26	Positive

[a] Log M: Concentration in well.
[b] Linear trend determines the relationship between ER-binding activity and UV influence exposed.

however, the ER-binding activity *significantly increased* ($p = 0.037$) compared to the parent compound. After the complete removal of BPA, most of the TPs were still observed (Fig. S8), suggesting little cytotoxic but potential estrogenic character of these TPs.

Compared to the parent compound DCF, the cytotoxicity *significantly decreased* ($p < 0.0001$) during the DCF degradation within 640 mJ cm^{-2} UV fluence. The ER-binding activity is significantly different ($p = 0.001$) following UV irradiation as shown in Fig. S16. ER-binding activity increased from 21.4% RME2 of non-irradiated sample to 63.6% RME2 at 40 mJ cm^{-2} UV fluence, subsequently and gradually decreased to 14.8% RME2 at 320 mJ cm^{-2} UV fluence, and increased again to 43.6% RME2 at 640 mJ cm^{-2} UV fluence. In particular, 1 μM DCF was completely decomposed after 320 mJ cm^{-2} UV fluence, suggesting possible declined cytotoxicity but enhanced estrogenic character of the TPs, such as D_{144}, and cyclization derivatives that could still be detected after the total removal of DCF (Fig. S9).

As IBP decomposed at 640 mJ cm^{-2} UV fluence, the cytotoxicity slightly *increased* ($p = 0.998$) and a non-significant *decrease* ($p = 0.151$) in ER-binding activity compared to the parent compound was observed, indicating the formed TPs did not contribute to higher cytotoxicity or estrogenic activity (Fig. S17).

The cytotoxicity of treated TCS slightly increased ($p = 0.813$) at 640 mJ cm^{-2} UV fluence compared to the parent compound as seen from Fig. S18. The estrogenic activity at 640 mJ cm^{-2} UV fluence decreased in a non-significant manner relative to parent compound ($p = 0.136$) with a negative linear trend between UV fluence and binding activity ($p = 0.034$). The results forecasted the decreasing trend of the estrogenic property of the resulting solution with UV irradiation in UV/H_2O_2 treatment, and the TPs (especially $T_{267\text{-}1}$) generated at low levels (Fig. S11) would not enhance the cytotoxicity or estrogenic activity.

Compared to the parent compound E1 (Fig. S19), the cytotoxicity decreased ($p = 0.625$) during the degradation of E1 at 640 mJ cm^{-2} UV fluence, and the ER-binding activity increased in a non-significant manner ($p = 0.542$) with a positive linear trend ($p = 0.262$). This result suggested the little cytotoxic but possible estrogenic character of the TPs formed (E_{285} and E_{301}) following E1 degradation in UV/H_2O_2 treatment.

3.4.2. Cytotoxicity and ER-binding activity of resulting solutions during the degradation of mixed CECs in UV/H_2O_2 treatment

Even though the mixed CECs in Milli-Q were completely removed by UV/H_2O_2 at 640 mJ cm^{-2} UV fluence as shown in Fig. S20a, considering the possible toxicity of excessive H_2O_2 and formed TPs, the UV irradiation time was extended to 3200 mJ cm^{-2}. A *decrease* ($p = 0.001$) of cytotoxicity in AhR cell line was observed in Fig. S20b. As shown in Fig. S20c, the cytotoxicity in ER cell line is significantly different following UV irradiation ($p = 0.044$), as the fraction survival decreased from 110.3% of non-irradiated sample to 65.9% of sample at 320 mJ cm^{-2} UV fluence but subsequently and gradually increased to 111.6% of sample at 3200 mJ cm^{-2} UV fluence. Meanwhile, the ER-binding activity significantly *decreased* ($p < 0.0001$, Fig. S21) compared to the solution containing the mixed parent compounds, indicating that higher UV fluence is necessary for UV/H_2O_2 treatment to reduce the cytotoxicity and estrogenic activity of the solution containing mixed CECs spiked at high concentrations.

RO permeate water samples were used with spiked chemicals (CECs and H_2O_2) to assess the resulting toxicity after the UV/H_2O_2 process. The cytotoxicity decreased ($p = 0.997$) compared to the parent compounds when the spiked CECs were decomposed by UV/H_2O_2 in RO I with 4800 mJ cm^{-2} UV fluence. The estrogenic properties of the spiked CEC mixture in the RO permeate during the UV/H_2O_2 process *increased* ($p = 0.286$) with a positive linear trend ($p = 0.130$) (Fig. S22) compared to the parent compounds. In future work, CECs at lower, environmentally relevant levels (100–200 ng L^{-1}) should be treated by UV/H_2O_2 (700–1000 mJ cm^{-2} UV fluence) and the toxicity should be assessed in order to determine whether there is any detectable toxicity and whether the trends observed in the present study are maintained. In general, little toxicity of MF/RO/UV-AOP product waters (non-spiked CECs) in potable reuse facilities was detected in other studies by measuring disinfection byproducts-associated toxicity (Chuang et al., 2019). Nevertheless, improvements in UV/H_2O_2 treatment may be beneficial to further reduce any measurable response from bioanalytical tools (which are highly sensitive indicators of cytotoxicity) during CEC degradation, as the formed TPs during UV/H_2O_2 are more toxic relative to their parent compounds.

Table 2
Cytotoxicity, ER-binding activity of CECs mixture during the LP-UV/H_2O_2 treatment in Milli-Q water and RO I. UV_{254nm} fluence rate = 0.1 mW cm^{-2}, $[CEC]_0$ = 1 μM, $[H_2O_2]_0$ = 1 mM, $pH_{endpoint}$ = 7.3, no buffer solutions. Endpoint for Milli-Q water was 3200 mJ cm^{-2} (8.89 h); and endpoint for RO I was 4800 mJ cm^{-2} (13.33 h).

Reaction Matrices	Cytotoxicity			ER-binding activity (log M = 0.5%)		ER-binding activity linear trend	
		p		p		p	
Milli-Q water	AhR cell line + MTT (log M = 1%)	0.001	*Decreased*	<0.0001	*Decreased*	–	Negative
	ER cell line + MTT (log M = 5%)	0.04	*Decreased*				
RO permeate	AhR cell line + MTT (log M = 5%)	0.997	*Decreased*	0.29	*Increased*	0.13	Positive

4. Conclusion

This study evaluated UV/H_2O_2 AOP for treatment of mixed CECs (BPA, E1, DCF, IBP, and TCS) including degradation kinetics, pathways, and resulting toxicity. First, the degradation rates of mixed CECs by LP-UV/H_2O_2 and LED-UV/H_2O_2 in Milli-Q water were similar, which were faster than that by UV only. ROS-oxidation primarily contributed to the destruction of BPA, E1, and IBP, while DCF and TCS were mainly decomposed by UV photolysis at 254 nm. ROS oxidation of CECs was significantly inhibited in the RO I, which posed little cytotoxicity and estrogenic activity compared to the blank. This inhibition phenomenon might be ascribed to the presence of certain LW-DOM at this facility or differences in the sewershed and wastewater discharges day-to-day, which deserves further investigation in the future.

Second, TPs were tentatively identified to better understand the toxicity of selected CECs during individual degradation by UV/H_2O_2 at 640 mJ cm^{-2}. For BPA degradation by UV/H_2O_2, hydroxylation and quinone products were detected; these showed little cytotoxicity but had higher estrogenic activity than BPA, which need to be isolated and assessed in the future. For DCF degradation, the cytotoxicity and estrogenic activity of resulting solutions were elevated, which might be ascribed to the generated hydroxylation and cyclization products. Even though many hydroxylation and decarboxylation IBP products were detected at relatively high levels during IBP degradation, the cytotoxicity did not change significantly and the estrogenic activity decreased slightly compared to the parent compound. During TCS degradation, dechlorination product T_{253b} was detected at a relatively high level and many other TPs were tentatively identified, including cyclization and dechlorination-hydroxylation products. However, the resulting cytotoxicity did not change significantly and the estrogenic activity declined slightly with a significant linear trend compared to TCS. As for E1 degradation, only three TPs were detected at relatively low levels with unchanged cytotoxicity; however, the estrogenic property increased, suggesting either $E_{285a\text{-}b}$ or E_{301} may be more estrogenic than E1.

Third, the toxicity of resulting solutions during the degradation of CEC mixtures by UV/H_2O_2 was considered, whether spiked in Milli-Q water or RO I. In Milli-Q water, both cytotoxicity and estrogenic activity significantly decreased during the degradation of the spiked CEC mixture by UV/H_2O_2 with high UV fluence (3200 mJ cm^{-2}). When CECs were spiked into RO permeate, the cytotoxicity and estrogenic properties were not entirely eliminated during degradation of mixed CECs by UV/H_2O_2 under current reaction conditions. Though the measurable toxicity is attributable to the relatively high (spiked) concentrations of the CECs used in the bioassay (15–150 μg L^{-1}) compared to the background concentrations detected in the RO permeate (influent into UV-AOP treatment, < 1 μg L^{-1}), the results still provide insights into the cytotoxicity and estrogenic activity of the selected CECs and their TPs during the UV/H_2O_2 process.

Declaration of competing interest

The authors declare that they have no known competing financial interests or personal relationships that could have appeared to influence the work reported in this paper.

Acknowledgements

The authors acknowledge financial support from the U.S. Geological Survey (USGS)-Water Resources Research Institute (WRRI) (2015SC101G) for this research. Ying Huang acknowledges support from the China Scholarship Council (CSC) scholarship (201306270057). Minghao Kong acknowledges support from the CSC scholarship (201608110134). We are thankful to Orange County Water District GWRS staffs for collecting and sending water samples used as a real-world reaction matrix and providing comments on manuscripts.

Appendix A. Supplementary data

Supplementary data to this article can be found online at https://doi.org/10.1016/j.watres.2020.115587.

References

Abdelraheem, W.H.M., Patil, M.K., Nadagouda, M.N., Dionysiou, D.D., 2019. Hydrothermal synthesis of photoactive nitrogen- and boron- codoped TiO_2 nanoparticles for the treatment of bisphenol A in wastewater: synthesis, photocatalytic activity, degradation byproducts and reaction pathways. Appl. Catal. B Environ. 241, 598–611.

Alharbi, S.K., Kang, J., Nghiem, L.D., van de Merwe, J.P., Leusch, F.D.L., Price, W.E., 2017. Photolysis and UV/H_2O_2 of diclofenac, sulfamethoxazole, carbamazepine, and trimethoprim: identification of their major degradation products by ESI–LC–MS and assessment of the toxicity of reaction mixtures. Process Saf. Environ. Protect. 112, 222–234.

Anderson, P., Denslow, N., Drewes, J., Olivieri, A., Schlenk, D., Snyder, S.A., 2010. Final Report: Monitoring Strategies for Chemicals of Emerging Concern (CECs) in Recycled Water. *Recommendations of a Science Advisory Panel* Convened by the California State Water Resources Control Board, Sacramento, Calif.

Appiani, E., Page, S.E., McNeill, K., 2014. On the use of hydroxyl radical kinetics to assess the number-average molecular weight of dissolved organic matter. Environ. Sci. Technol. 48 (20), 11794–11802.

Binz, C., Harris-Lovett, S., Kiparsky, M., Sedlak, D.L., Truffer, B., 2016. The thorny road to technology legitimation - institutional work for potable water reuse in California. Technol. Forecast. Soc. Change 103, 249–263.

Bolton, J., Beck, S., Linden, K., 2015. Protocol for the determination of fluence (UV dose) using a low-pressure or low-pressure high-output UV lamp in bench-scale collimated beam ultraviolet experiments. IUVA News 17, 11–17.

Chuang, Y.-H., Chen, S., Chinn, C.J., Mitch, W.A., 2017. Comparing the UV/monochloramine and UV/free chlorine advanced oxidation processes (AOPs) to the UV/hydrogen peroxide AOP under scenarios relevant to potable reuse. Environ. Sci. Technol. 51 (23), 13859–13868.

Chuang, Y.-H., Szczuka, A., Mitch, W.A., 2019. Comparison of toxicity-weighted disinfection byproduct concentrations in potable reuse waters and conventional drinking waters as a new approach to assessing the quality of advanced treatment train waters. Environ. Sci. Technol. 53 (7), 3729–3738.

de Luna, L.A.V., da Silva, T.H.G., Nogueira, R.F.P., Kummrow, F., Umbuzeiro, G.A., 2014. Aquatic toxicity of dyes before and after photo-Fenton treatment. J. Hazard Mater. 276, 332–338.

Dhara, A.K., Singh, U.P., Ghosh, K., 2016. Radical pathways and O_2 participation in benzyl alcohol oxidation, and catechol and o-aminophenol oxidase activity studies with novel zinc complexes: an experimental and theoretical investigation. Inorg. Chem. Front. 3 (12), 1543–1558.

Escher, B.I., Allinson, M., Altenburger, R., Bain, P.A., Balaguer, P., Busch, W., Crago, J., Denslow, N.D., Dopp, E., Hilscherova, K., Humpage, A.R., Kumar, A., Grimaldi, M., Jayasinghe, B.S., Jarosova, B., Jia, A., Makarov, S., Maruya, K.A., Medvedev, A., Mehinto, A.C., Mendez, J.E., Poulsen, A., Prochazka, E., Richard, J., Schifferli, A., Schlenk, D., Scholz, S., Shiraishi, F., Snyder, S., Su, G., Tang, J.Y.M., Burg, B.v.d., Linden, S.C.v.d., Werner, I., Westerheide, S.D., Wong, C.K.C., Yang, M., Yeung, B.H.Y., Zhang, X., Leusch, F.D.L., 2014. Benchmarking organic micropollutants in wastewater, recycled water and drinking water with in vitro bioassays. Environ. Sci. Technol. 48 (3), 1940–1956.

Gao, Y., Ji, Y., Li, G., An, T., 2014. Mechanism, kinetics and toxicity assessment of OH-initiated transformation of triclosan in aquatic environments. Water Res. 49, 360–370.

Gligorovski, S., Strekowski, R., Barbati, S., Vione, D., 2015. Environmental implications of hydroxyl radicals (•OH). Chem. Rev. 115 (24), 13051–13092.

Hach Company, H.L.G., 2014. Chloramine. Mono, USA.

He, X., Pelaez, M., Westrick, J.A., O'Shea, K.E., Hiskia, A., Triantis, T., Kaloudis, T., Stefan, M.I., de la Cruz, A.A., Dionysiou, D.D., 2012. Efficient removal of microcystin-LR by UV-C/H_2O_2 in synthetic and natural water samples. Water Res. 46 (5), 1501–1510.

He, X., Zhang, G., de la Cruz, A.A., O'Shea, K.E., Dionysiou, D.D., 2014. Degradation mechanism of cyanobacterial toxin cylindrospermopsin by hydroxyl radicals in homogeneous UV/H_2O_2 process. Environ. Sci. Technol. 48 (8), 4495–4504.

Huang, Y., Han, C., Liu, Y., Nadagouda, M.N., Machala, L., O'Shea, K.E., Sharma, V.K., Dionysiou, D.D., 2018a. Degradation of atrazine by $Zn_xCu_{1-x}Fe_2O_4$ nanomaterial-catalyzed sulfite under UV–vis light irradiation: green strategy to generate $SO_4^{\bullet-}$. Appl. Catal. B Environ. 221 (Suppl. C), 380–392.

Huang, Y., Kong, M., Westerman, D., Xu, E.G., Coffin, S., Cochran, K.H., Liu, Y., Richardson, S.D., Schlenk, D., Dionysiou, D.D., 2018b. Effects of HCO_3^- on degradation of toxic contaminants of emerging concern by UV/NO_3^-. Environ. Sci. Technol. 52 (21), 12697–12707.

Huang, Y., Liu, Y., Kong, M., Xu, E.G., Coffin, S., Schlenk, D., Dionysiou, D.D., 2018c. Efficient degradation of cytotoxic contaminants of emerging concern by UV/H_2O_2. Environ. Sci.: Water Res. & Tech.

Kang, Y.-M., Kim, M.-K., Zoh, K.-D., 2018. Effect of nitrate, carbonate/bicarbonate, humic acid, and H_2O_2 on the kinetics and degradation mechanism of bisphenol-A during UV photolysis. Chemosphere 204, 148–155.

Kliegman, S., Eustis, S.N., Arnold, W.A., McNeill, K., 2013. Experimental and theoretical insights into the involvement of radicals in triclosan phototransformation. Environ. Sci. Technol. 47 (13), 6756–6763.

Kwon, M., Kim, S., Jung, Y., Hwang, T.-M., Stefan, M.I., Kang, J.-W., 2019. The impact of natural variation of oh radical demand of drinking water sources on the optimum operation of the UV/H_2O_2 process. Environ. Sci. Technol. 53 (6), 3177–3186.

Latch, D.E., Packer, J.L., Arnold, W.A., McNeill, K., 2003. Photochemical conversion of triclosan to 2,8-dichlorodibenzo-p-dioxin in aqueous solution. J. Photochem. Photobiol. Chem. 158 (1), 63–66.

Li, H., Long, Y., Zhu, X., Tian, Y., Ye, J., 2017. Influencing factors and chlorinated byproducts in electrochemical oxidation of bisphenol A with boron-doped diamond anodes. Electrochim. Acta 246, 1121–1130.

Li, W., Xu, E., Schlenk, D., Liu, H., 2018. Cyto- and geno-toxicity of 1,4-dioxane and its transformation products during ultraviolet-driven advanced oxidation processes. Environ. Sci.: Water Res. & Technol. 4 (9), 1213–1218.

Mariani, M.L., Romero, R.L., Zalazar, C.S., 2015. Modeling of degradation kinetic and toxicity evaluation of herbicides mixtures in water using the UV/H_2O_2 process. Photochem. Photobiol. Sci. 14 (3), 608–617.

Maruya, K.A., Schlenk, D., Anderson, P.D., Denslow, N.D., Drewes, J.E., Olivieri, A.W., Scott, G.I., Snyder, S.A., 2014. An adaptive, comprehensive monitoring strategy for chemicals of emerging concern (CECs) in California's aquatic ecosystems. Integrated Environ. Assess. Manag. 10 (1), 69–77.

Mezcua, M., Gómez, M.J., Ferrer, I., Aguera, A., Hernando, M.D., Fernández-Alba, A.R., 2004. Evidence of 2,7/2,8-dibenzodichloro-p-dioxin as a photodegradation product of triclosan in water and wastewater samples. Anal. Chim. Acta 524 (1), 241–247.

Moussavi, G., Pourakbar, M., Shekoohiyan, S., Satari, M., 2018. The photochemical decomposition and detoxification of bisphenol A in the VUV/H_2O_2 process: degradation, mineralization, and cytotoxicity assessment. Chem. Eng. J. 331, 755–764.

Munoz, M., de Pedro, Z.M., Casas, J.A., Rodriguez, J.J., 2012. Triclosan breakdown by Fenton-like oxidation. Chem. Eng. J. 198–199, 275–281.

Musa, K.A.K., Eriksson, L.A., 2009. Photodegradation mechanism of the common non-steroid anti-inflammatory drug diclofenac and its carbazole photoproduct. Phys. Chem. Chem. Phys. 11 (22), 4601–4610.

Olmez-Hanci, T., Dursun, D., Aydin, E., Arslan-Alaton, I., Girit, B., Mita, L., Diano, N., Mita, D.G., Guida, M., 2015. $S_2O_8^{2-}$/UV-C and H_2O_2/UV-C treatment of bisphenol A: assessment of toxicity, estrogenic activity, degradation products and results in real water. Chemosphere 119, S115–S123.

Patton, S., Romano, M., Naddeo, V., Ishida, K.P., Liu, H., 2018. Photolysis of mono- and dichloramines in UV/hydrogen peroxide: Effects on 1,4-dioxane removal and relevance in water reuse. Environ. Sci. Technol. 52 (20), 11720–11727.

Pérez-Estrada, L.A., Malato, S., Gernjak, W., Agüera, A., Thurman, E.M., Ferrer, I., Fernández-Alba, A.R., 2005. Photo-Fenton degradation of diclofenac: Identification of main intermediates and degradation pathway. Environ. Sci. Technol. 39 (21), 8300–8306.

Rogers, J.M., Denison, M.S., 2000. Recombinant cell bioassays for endocrine disruptors: development of a stably transfected human ovarian cell line for the detection of estrogenic and anti-estrogenic chemicals. In Vitr. Mol. Toxicol. 13 (1), 67–82.

Sein, M.M., Zedda, M., Tuerk, J., Schmidt, T.C., Golloch, A., von Sonntag, C., 2008. Oxidation of diclofenac with ozone in aqueous solution. Environ. Sci. Technol. 42 (17), 6656–6662.

Shu, Z., Singh, A., Klamerth, N., McPhedran, K., Bolton, J.R., Belosevic, M., Gamal El-Din, M., 2016. Pilot-scale UV/H_2O_2 advanced oxidation process for municipal reuse water: assessing micropollutant degradation and estrogenic impacts on goldfish (Carassius auratus L.). Water Res. 101, 157–166.

Van de Loosdrecht, A.A., Beelen, R.H.J., Ossenkoppele, G.J., Broekhoven, M.G., Langenhuijsen, M.M.A.C., 1994. A tetrazolium-based colorimetric MTT assay to quantitate human monocyte mediated cytotoxicity against leukemic cells from cell lines and patients with acute myeloid leukemia. J. Immunol. Methods 174 (1), 311–320.

Vogna, D., Marotta, R., Napolitano, A., Andreozzi, R., d'Ischia, M., 2004. Advanced oxidation of the pharmaceutical drug diclofenac with UV/H_2O_2 and ozone. Water Res. 38 (2), 414–422.

Wols, B.A., Hofman-Caris, C.H.M., Harmsen, D.J.H., Beerendonk, E.F., 2013. Degradation of 40 selected pharmaceuticals by UV/H_2O_2. Water Res. 47 (15), 5876–5888.

Wooding, K.M., Barkley, R.M., Hankin, J.A., Johnson, C.A., Bradford, A.P., Santoro, N., Murphy, R.C., 2013. Mechanism of formation of the major estradiol product ions following collisional activation of the molecular anion in a tandem quadrupole mass spectrometer. J. Am. Soc. Mass Spectrom. 24 (10), 1451–1455.

Wu, Z., Fang, J., Xiang, Y., Shang, C., Li, X., Meng, F., Yang, X., 2016. Roles of reactive chlorine species in trimethoprim degradation in the UV/chlorine process: kinetics and transformation pathways. Water Res. 104, 272–282.

Yin, K., Deng, L., Luo, J., Crittenden, J., Liu, C., Wei, Y., Wang, L., 2018. Destruction of phenicol antibiotics using the UV/H_2O_2 process: kinetics, byproducts, toxicity evaluation and trichloromethane formation potential. Chem. Eng. J. 351, 867–877.

Zhang, Z., Chuang, Y.-H., Szczuka, A., Ishida, K.P., Roback, S., Plumlee, M.H., Mitch, W.A., 2019. Pilot-scale evaluation of oxidant speciation, 1,4-dioxane degradation and disinfection byproduct formation during UV/Hydrogen peroxide, UV/Free chlorine and UV/Chloramines advanced oxidation process treatment for potable reuse. Water Res. 164, 114939.